Direct Synthesis of Photocatalytically Active Rutile TiO2 Nanorods Partly Decorated with Anatase Nanoparticles

ARTICLE *in* THE JOURNAL OF PHYSICAL CHEMISTRY C · MARCH 2010

Impact Factor: 4.77 · DOI: 10.1021/Jp912008k

4 AUTHORS, INCLUDING:

Tarek A. Kandiel
Faculty of Science, Sohag University
22 PUBLICATIONS **551** CITATIONS
SEE PROFILE

Armin Feldhoff
Leibniz Universität Hannover
140 PUBLICATIONS **3,997** CITATIONS
SEE PROFILE

Direct Synthesis of Photocatalytically Active Rutile TiO_2 Nanorods Partly Decorated with Anatase Nanoparticles

Tarek A. Kandiel,[†] Ralf Dillert,[†] Armin Feldhoff,[‡] and Detlef W. Bahnemann*,[†]

Institut für Technische Chemie, Leibniz Universität Hannover, Callinstrasse 3, D-30167 Hannover, Germany, and Institut für Physikalische Chemie und Elektrochemie, Leibniz Universität Hannover, Callinstrasse 3a, D-30167 Hannover, Germany

Received: December 20, 2009; Revised Manuscript Received: February 7, 2010

TiO_2 rutile nanorods either decorated with anatase nanoparticles or pure have been prepared via a facile single-step hydrothermal method using commercially available aqueous solutions of titanium bis(ammonium lactate) dihydroxide at natural pH (∼8.0) without any additives. The obtained powders have been characterized by X-ray diffraction, field-emission scanning electron microscopy, high-resolution transmission electron microscopy, UV−vis diffuse reflectance spectroscopy, and nitrogen adsorption. The photocatalytic activities have been evaluated for the gas-phase decomposition of acetaldehyde under UV(A) illumination. The results revealed that TiO_2 rutile nanorods decorated with anatase nanoparticles exhibit a higher photocatalytic activity than those embedded in anatase nanoparticles or without any anatase contact. This behavior is explained by the better charge carrier separation in the case of anatase rutile mixtures.

Introduction

TiO_2 nanomaterials with different morphologies and polymorphs have recently attracted great interest, as their optical and electrical properties strongly depend on shape, size, and phase composition.[1] It is well-known that crystalline TiO_2 exists in three polymorphs: anatase, rutile, and brookite. Among them, the rutile polymorph exhibits an excellent combination of physical properties that has made it worldwide the most widely used white pigment as a result of its exceptional light scattering efficiency, its high refractive index, its opacity, and its chemical inertness. As a photocatalyst rutile has in most cases been shown to exhibit a lower photocatalytic activity than anatase;[2] however, in some cases the activity has been found to be superior.[3] Synergistic effects between anatase and rutile nanoparticles leading to spatial charge separation and hindered recombination have been proposed to explain the enhanced photocatalytic efficiency of anatase and rutile mixed phases.[4]

The synthesis of rutile TiO_2 nanocrystals, unlike anatase, is much more difficult because most of the methods adopted for the synthesis of TiO_2 generally produce the kinetically controlled structure, i.e, anatase, at low temperatures.[5] Several studies, however, have been dedicated to the exploration of novel methods for the preparation of rutile TiO_2 nanorods. In most cases, $TiCl_4$, $TiCl_3$, or titanium alkoxides have been used as precursors in highly acidic medium and/or in the presence of additives, e.g, surfactants, organic acids, mineralizers, and seeds.[6] However, the hydrolysis of $TiCl_4$ and titanium alkoxides will inevitably take place in water, even in moist air. Therefore, ice-cooled water baths are often used to ensure a control of the experiments. Hence, it is challenging to develop a simple one-step method for the preparation of rutile TiO_2 nanorods in an aqueous environment at low temperatures. To the best of our knowledge, only a few reports have so far been published focusing on the synthesis of rutile nanorods from adequate precursors in the aqueous phase;[7] however, the precursors were self-prepared and different additives had to be employed during the synthesis. Also, only one report has presented a method for the decoration of rutile TiO_2 nanorods by anatase nanoparticles employing, however, a highly sophisticated layer-by-layer assembly technique.[8] Here, for the first time, the synthesis of rutile TiO_2 nanorods decorated with anatase nanoparticles as well as that of pure rutile nanorods is reported employing a facile single-step hydrothermal method starting from commercially available aqueous solutions of titanium bis(ammonium lactate) dihydroxide (TALH) at natural pH (∼8.0) without requiring any other additives.

Experimental Section

Hydrothermal Synthesis. Thermal hydrolysis experiments were carried out in a 200 mL Teflon cup enclosed in a stainless steel autoclave (Berghof, DAB-3). In a typical experiment, 10 mL of TALH aqueous precursor (50%, Sigma-Aldrich) and 40 mL of deionized water were mixed. The resulting solution was transferred into the Teflon cup. Afterward, the Teflon cup was sealed in the autoclave and placed into an electric furnace held at 200 °C for a required time. Then, the autoclave was cooled in air at ambient temperature. The resulting powders were separated from the remaining liquids by centrifugation, sonicated, and washed several times with water until a clear supernatant solution was obtained, followed by drying overnight at 60 °C.

Characterization. X-ray diffraction (XRD) data for the Rietveld phase analysis of TiO_2 have been recorded on a Phillips PW1800 diffractometer using a reflection geometry with variable divergence slits, Cu $K\alpha_{1,2}$ radiation, and a secondary monochromator. For each measurement 3000 data points were collected with a step width of 0.02° and 2 s measurement time per step in the 2θ range from 20 to 80°. Phase analysis by the Rietveld method was carried out by using the TOPAS 2.0 (Bruker AXS) software. During the computational refinements general parameters such as scale factors, one background

* To whom correspondence should be addressed. Telephone: +49-511-762-5560. Fax: +49-511-762-2774. E-mail: bahnemann@iftc.uni-hannover.de.
[†] Institut für Technische Chemie.
[‡] Institut für Physikalische Chemie und Elektrochemie.

10.1021/jp912008k
Published on Web 02/25/2010

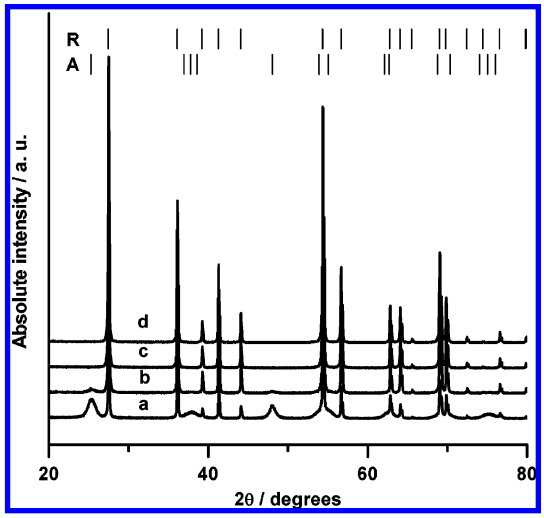

Figure 1. XRD patterns of as-synthesized nanocrystalline TiO_2 powders obtained by thermal hydrolysis of aqueous solutions of the TALH precursor at 200 °C for (a) 24, (b) 48, (c) 72, and (d) 96 h. Labels "R" and "A" indicate Bragg positions for rutile and anatase, respectively.

parameter, and the zero point error were optimized. Profile shape calculations were carried out on the basis of standard instrumental parameters using the fundamental parameter approach implemented in the program and varying the average crystal size (integral breadth) of the reflections. Lattice parameters and crystallite size of all phases were refined. Structural data for the known phases were taken from the PDF-2 database with PDF numbers: anatase, 21-1272; rutile, 21-1276; and brookite, 29-1360.

Brunauer−Emmett−Teller (BET) surfaces have been estimated by single-point standard surface area measurements employing a Micromeritics FlowSorb II 2300 instrument equipped with Micromeritics AutoMate 23. The gas mixture used for the adsorption and desorption measurements consisted of 30% N_2 and 70% He. The TiO_2 samples were previously heated to 150 °C for approximately 60 min in order to clean the surface from adsorbed organic compounds and water.

Field-emission scanning electron microscopy (FE-SEM) measurements were carried out employing a JEOL JSM-6700F field-emission instrument and using a secondary electron detector (SE) at an accelerating voltage of 2 kV. High-resolution transmission electron microscopy (HRTEM) was performed at 200 kV on a field-emission instrument of the type JEM-2100F (JEOL Ltd., Tokyo, Japan) with an ultrahigh-resolution pole piece (CS = 0.5 mm, CS = 1.2 mm), providing a point resolution better than 0.19 nm. Sample preparation was made by dispersing the powder in ethanol and dropping ca. 10 μL of the suspension onto a copper-supported perforated carbon film of the type Multi A (Quantifoil Micro Tools GmbH, Jena, Germany), on which it was dried. Observation of powder particles was made in specimen areas, which were locally not supported by the carbon film.

A Varian Cary 100 Scan UV−visible system equipped with a labsphere diffuse reflectance accessory was used to obtain the reflectance spectra of the powder over a range of 200−800 nm. Labsphere USRS-99-010 was employed as a reflectance standard.

Photocatalytic Activity. Photocatalytic decomposition of gaseous acetaldehyde was carried out in an experimental setup consisting of a gas supply, the photoreactor, and a gas chromatograph for acetaldehyde analysis (GC 955 Syntech Spectras). To obtain the starting concentration of acetaldehyde of 1 ppm at a relative humidity of 50%, a gaseous mixture of dry air (500 mL min^{-1}), wet air (500 mL min^{-1}, relative humidity 100%), and acetaldehyde (6 mL min^{-1}) was prepared. This gas stream was continuously flowed through the photoreactor, and photocatalytic oxidation of acetaldehyde was obtained over TiO_2 films with a geometric area of about 30 cm^2 and UV light with an intensity of 1 mW cm^{-2} and a mean wavelength of $\lambda = 350$ nm. The TiO_2 films were prepared by mixing 1 mL of water and 100 mg of TiO_2 powder homogeneously by sonication. This TiO_2 suspension was spread on a glass with a glass rod, using adhesive tapes as spacers, and was then allowed to dry in air at 100 °C for 2 h.

Results

Titanium dioxide nanoparticles have been prepared by the thermal hydrolysis of aqueous solutions of the TALH complex at 200 °C for 24, 48, 72, and 96 h. Figure 1 shows the XRD patterns of the isolated powders obtained after the different reaction times. Clearly, all the diffraction patterns can be indexed to the anatase and the rutile phases, respectively. With increasing reaction time, the peaks assigned to the anatase phase completely disappear and pure rutile is found after 72 and 96 h of hydrothermal treatment (Figure 1c,d). The quantitative phase composition and crystallite diameter of nanocrystalline TiO_2 powders as evident from the Rietveld analysis of the XRD data are given in Table 1. The Brunauer−Emmett−Teller (BET) specific surface area, the pH measured at the end of the synthesis, and the yield are also summarized in Table 1. The yield has been calculated relative to the expected yield upon complete thermal hydrolysis of the TALH complex regardless of the possible losses resulting from the washing process.

The morphology of the isolated powders has been investigated by field-emission scanning electron microscopy (FE-SEM). The micrographs of the TiO_2 powders obtained by thermal hydrolysis of aqueous solutions of TALH at 200 °C for 24 h (RA24) and 48 h (RA48) indicate the formation of rodlike particles either embedded in or decorated with small nanoparticles as shown in parts a and b, respectively, of Figure 2. Upon further increase of the reaction time to 72 and 96 h, only the rodlike particles are obtained as shown in Figure 2c,d (named R72 and R96, respectively). At this point, it should be emphasized that the

TABLE 1: Quantitative Phase Composition, Crystallite Diameter, BET Surface Area, Yield of Nanocrystalline TiO_2 Prepared by Thermal Hydrolysis of the TALH Precursor at 200 °C, and pH Measured after Termination of the Synthesis

reaction time (h)	anatase (%)	anatase crystallite size (nm)	rutile (%)	rutile crystallite size (nm)	BET surface area (m^2 g^{-1})	yield (%)	final pH
24	53	10	47	118	92	100[a]	5.0
48	9	11	91	145	16	90	5.3
72	0	0	100	147	6	96	5.5
96	0	0	100	152	6	96	6.0

[a] Isolated powder without washing cycles.

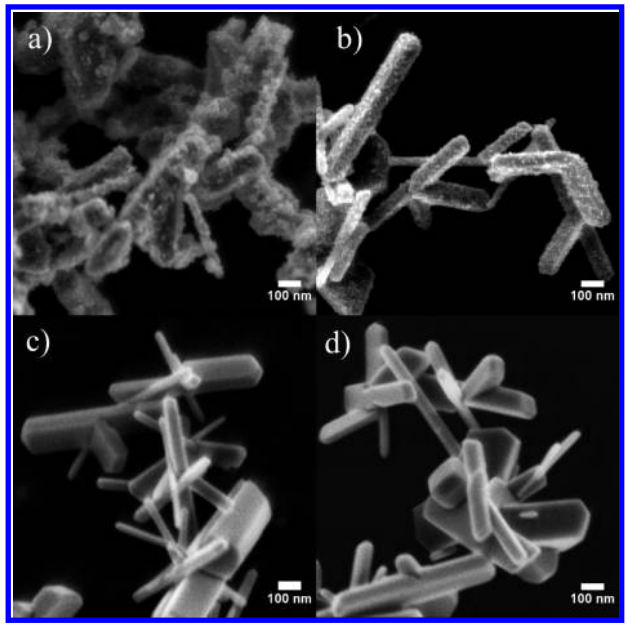

Figure 2. FE-SEM micrographs of as-synthesized nanocrystalline TiO_2 powders obtained by thermal hydrolysis of aqueous solutions of the TALH precursor at 200 °C for (a) 24, (b) 48, (c) 72, and (d) 96 h.

small nanoparticles adhere strongly to the surface of the rodlike nanoparticles as they cannot be removed even by sonication and several washing cycles. Depending on the crystallite size obtained from XRD analysis and the particle morphology observed in the SEM micrographs, it can be concluded that the small nanoparticles should be anatase whereas the nanorods should be rutile. However, by definition, the crystallite size calculated from XRD analysis does not necessarily match the particle size as seen by SEM.

The high-resolution TEM micrographs of the powder obtained after 48 h of hydrothermal treatment are shown in Figure 3. It is obvious from Figure 3b that the surfaces of the rutile nanorods are decorated by smaller equiaxial particles of 3−5 nm in diameter. In Figure 3c some of the smaller particles appear by bright contrast due to strong diffraction of electrons into the 15 mrad opening of the dark-field aperture. Thus, the crystalline nature of the smaller TiO_2 nanoparticles is proved. The rutile nanorods are elongated along their *c*-axis and show microfacets of the $(1\bar{1}1)$, $(1\bar{1}2)$, and (001) types at their tips as illustrated by the lines in the high-resolution micrograph in Figure 4b and the inset in Figure 4a. The high-resolution TEM micrograph in Figure 4c shows the rutile lattice along the (001) zone axis. The corresponding Fourier transform (Figure 4d) confirms the orientation of the rutile rod. Hence, the rutile particles have grown into rods along the *c*-axis (001) direction and exhibit primarily (110)-type facets. A schematic sketch of the rutile shape is given in Figure 4e. The SEM and TEM micrographs show that the diameter of the rutile rods varies from 50 to 100 nm and the length from 500 to 700 nm (Figures 2 and 3). Rutile nanorods of the same shape and with microfacets at their tips have been previously observed in some commercial TiO_2 powders,[9] however, with a much smaller size. A particular different situation is on the other hand given here by the decoration of the surface of the rutile nanorods by very small equiaxial TiO_2 nanoparticles.

The optical properties of the titania powders prepared here were determined using UV−vis diffuse reflectance spectroscopy as shown in Figure 5(left). It is clear from the onset of the absorbance (the Kubelka−Munk function $F(R)$ is equivalent to absorbance) in Figure 5(left) that the presence of anatase nanoparticles does not affect the optical properties of rutile nanorods. Since TiO_2 has an indirect electronic transition at the onset of absorption, the band gap energy was estimated by plotting the modified Kubelka−Munk function $[F(R)E]^{1/2}$ vs the energy of the exciting light E as shown in Figure 5(right).[10] The intercept of the linear fit with the *x*-axis yields a band gap energy of 3.0 eV for all materials prepared here, in good agreement with the value usually quoted for rutile TiO_2.

The photocatalytic activities of all materials prepared here were evaluated by the decomposition of gaseous acetaldehyde. The photonic efficiency ζ, which is defined as the ratio of the degradation rate of acetaldehyde and the incident photon flux (calculated for the mean irradiation wavelength of 350 nm and the employed light intensity) related to the illuminated area, was calculated according to

$$I_0 = \frac{I\lambda}{N_A hc}$$

$$\zeta\,(\%) = \frac{\Delta \cdot n_{\text{acetaldehyde}}}{I_0 A} 100$$

(with I_0 = light flux (einstein s^{-1} cm^{-2}); I = light intensity (J s^{-1} cm^{-2}); N_A = Avogadro's number (mol^{-1}); h = Planck's constant (J s); c = light velocity (m s^{-1}); λ = wavelength (m); $\Delta \cdot n_{\text{acetaldehyde}}$ is the difference between inlet and outlet fluxes of acetaldehyde (mol s^{-1}); A is the illuminated area of the TiO_2 film (cm^2)).

Under the present experimental conditions, TiO_2 films coated on glass substrates were employed during the photocatalytic decomposition of gaseous acetaldehyde. These TiO_2 films are thick enough (average thickness 7.0 μm) to ensure that no light is transmitted. Therefore, the incident light is completely absorbed by the TiO_2 films except for the fraction of light that is backscattered. Depending on the diffuse reflectance measurements (cf. Figure 5(left)), it is reasonable to assume that the fraction of the backscattered light is almost identical for all photocatalysts synthesized here. Thus, the photonic efficiencies were calculated assuming the investigated powders absorb the same amount of light. With the illumination area A = 30 cm^2, the complete degradation of all incoming acetaldehyde with an initial concentration of 1 ppm, which corresponds to $\Delta \cdot n_{\text{acetaldehyde}} = 6.76 \times 10^{-10}$ mol s^{-1}, results in a maximum achievable photonic efficiency ζ_{th} of 0.77%. All efficiencies of the analyzed samples were calculated after 120 min illumination time to ensure steady-state behavior and to avoid adsorption/desorption effects. Figure 6 shows the photonic efficiencies of the rutile nanorods either embedded in (RA24) or decorated with anatase nanoparticles (RA48) and those of the pure rutile nanorods (R72 and R96). For comparison, the photonic efficiencies of TiO_2 Evonik Aeroxide P25 (P25) and commercial rutile TiO_2 nanoparticles powders (supplied by Crystal Global Chemicals, Grimsby, U.K.) are also presented. The rutile nanoparticles powders have particle sizes of 25 and 34 nm and BET surface areas of 42 and 33 m^2 g^{-1}, respectively (denoted as R25 and R34, respectively).

Discussion

Proposed Formation Route of TiO_2 Rutile Nanorods. The observed formation of rutile nanorods decorated with anatase nanoparticles and of pure rutile nanorods by hydrothermal

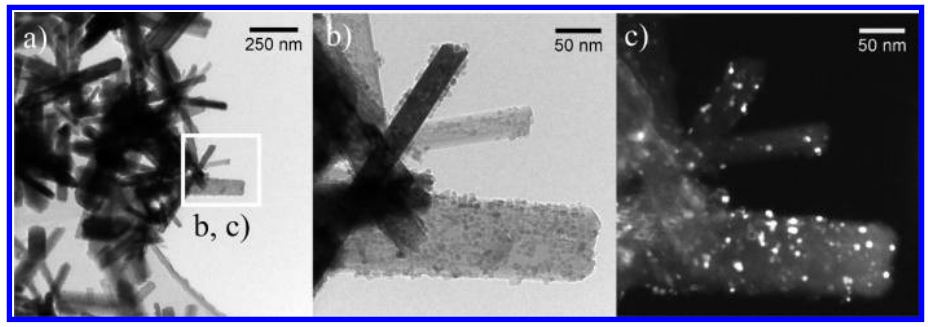

Figure 3. High-resolution transmission electron micrographs of as-synthesized nanocrystalline TiO_2 powder obtained by thermal hydrolysis of aqueous solutions of the TALH precursor for 48 h: (a) TEM bright-field, low magnification, (b) TEM bright-field, high magnification, and (c) TEM dark field.

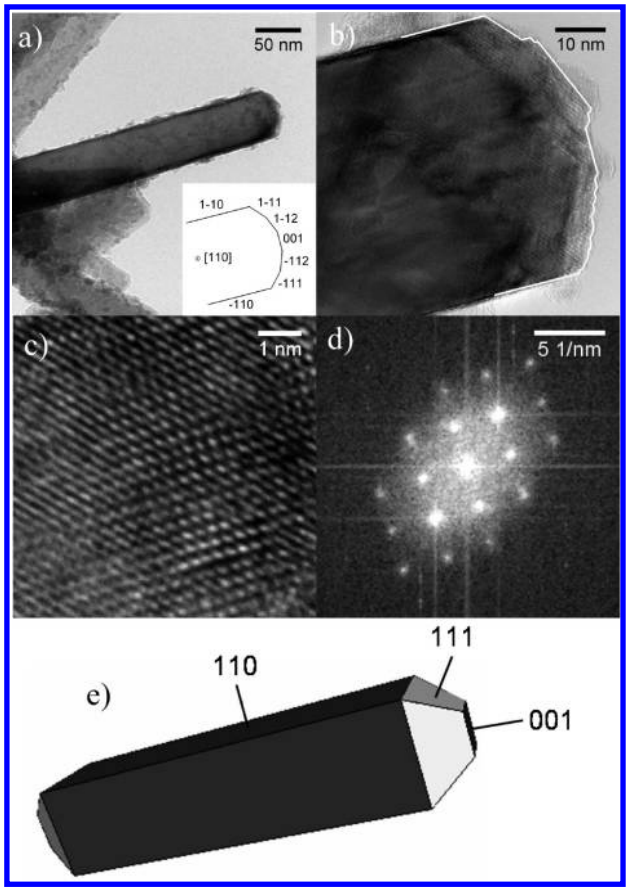

Figure 4. Shape analysis of as-synthesized nanocrystalline TiO_2 powder obtained by thermal hydrolysis of aqueous solutions of the TALH precursor for 48 h: (a) TEM bright-field micrograph, (b, c) high-resolution TEM micrographs, (d) Fourier transform of (c), and (e) sketch of the shape.

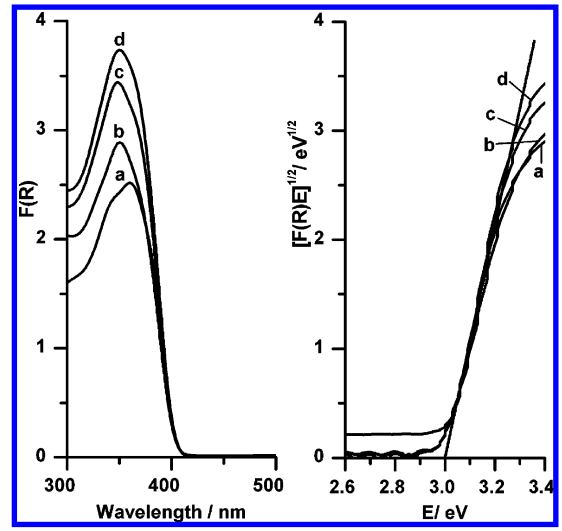

Figure 5. (left) Diffuse reflectance spectra of as-synthesized nanocrystalline TiO_2 powders obtained by thermal hydrolysis of aqueous solutions of the TALH precursor at 200 °C for (a) 24, (b) 48, (c) 72, and (d) 96 h. (right) Plot of the modified Kubelka−Munk function versus the energy of light absorbed.

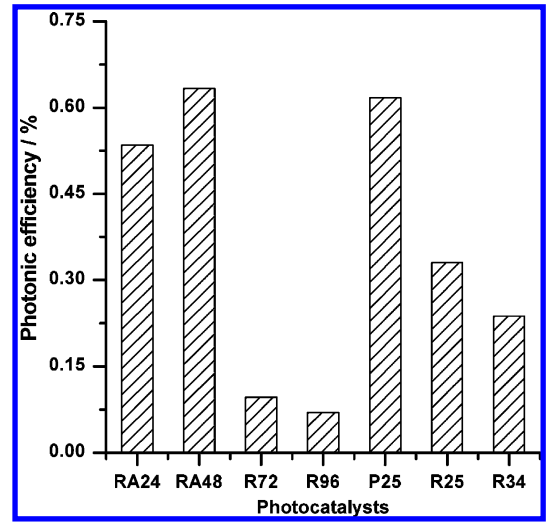

Figure 6. Comparison of photocatalytic activities of rutile nanorods decorated with anatase nanoparticles and of pure rutile nanorods obtained after different hydrothermal reaction times.

treatment of aqueous solutions of the TALH complex at 200 °C for different reaction times (24, 48, 72, and 96 h) is in contrast to published results. Möckel et al.[11] observed the formation of anatase TiO_2 nanoparticles during the thermal hydrolysis of the TALH complex at slightly different conditions, i.e., employing sealed glass ampules or a titanium autoclave.[12] They noted that characteristic rutile needles are formed besides these anatase nanoparticles only when the thermal hydrolysis experiment was performed at temperatures around 400 °C in the latter. An effect of the reaction time on the crystal size of the anatase nanoparticles was only observed at the beginning of the reaction at temperatures below 300 °C. In the present work, the XRD data (Figure 1) clearly show that biphasial anatase and rutile mixtures are already formed after 24 and 48 h of hydrothermal treatment of the TALH complex at 200 °C. At longer reaction times (72 and 96 h), only the pure rutile polymorph is obtained (cf. Figure 1c,d). These results indicate that there is a phase transformation from anatase nanoparticles to rutile nanorods with an increase of the reaction time. The hydrothermal treatment of rutile-free anatase TiO_2 nanoparticles at 200 °C in the presence of ammonium lactate (a product

expected from the thermal hydrolysis of TALH complex) resulted only in an increase of the size of the nanoparticles but not in a direct transformation of anatase to rutile (data not shown). From this experiment, it can be concluded that under the applied experimental conditions it is unlikely for anatase to transform to rutile without rutile nuclei being present. It has been reported that the presence of rutile seeds accelerates the crystallization of TiO_2, making the formation reaction of rutile kinetically more favorable than the formation of anatase during the hydrolysis of $TiCl_4$ at low temperature.[13] It is also important to mention that the hydrothermal treatment of the TALH complex for shorter times (12 h) or at lower temperature (120 °C) leads to the formation of stable suspensions of TiO_2 nanoparticles. It is therefore assumed that small anatase and rutile TiO_2 nuclei covered with lactate anions as hydroxycarboxylate ligands are formed at the early stage of the reaction. Recently, a similar behavior was reported by Kakihana and coworkers,[7] who obtained pure rutile TiO_2 by hydrothermal treatment of aqueous solutions of the titanium glycolate complex at 200 °C for reaction times exceeding 24 h whereas mixtures of anatase and rutile TiO_2 were obtained at 160 °C (24 h reaction time) and at 200 °C (6 h reaction time).

Depending on the experimental results of the present work, the proposed formation routes of the rutile TiO_2 nanorods are schematically given in Figure 7: (1) condensation−dehydration reaction between the −OH ligands forming Ti−O−Ti oxo species; (2) competing formation of anatase and rutile seeds; (3) anisotropic growth of the rutile TiO_2 seeds as the thermodynamically more stable phase, accompanied by the consumption of the small anatase TiO_2 nanoparticles. The anisotropic crystal growth along the *c*-axis (001) direction of the rutile TiO_2 seeds leads to the formation of rutile nanorods with primarily (110)-type facets as confirmed by TEM analysis. This can be explained by the well-established fact that during crystal growth a fast growing plane with a high surface energy tends to disappear, leaving behind slower growing planes with lower surface energies. It is known that the (110) plane of rutile TiO_2 has the lowest surface energy whereas the (001) plane has the highest surface energy.[14] Additionally, the anisotropic crystal growth observed during the thermal hydrolysis of the TALH complex might be facilitated by the presence of lactate anions acting as chelating ligands attached to the surfaces of the nanoparticles and thus possibly inhibiting the growth along other crystallographic directions.[15] Similar preferential growth of rutile nanorods along the *c*-axis has previously been reported.[16]

As observed in the FE-SEM and HR-TEM micrographs (Figures 2 and 3), the rutile nanorods obtained after 24 and 48 h of hydrothermal treatment are either embedded in or decorated with anatase nanoparticles (3−5 nm). These anatase nanoparticles adhere strongly to the surface of the rutile nanorods. In the case of rutile nanorods embedded in anatase nanoparticles (RA24), it is possible to remove all excess anatase nanoparticles by washing which, however, does not remove the anatase nanoparticles adhering at the rutile surface. The strong interaction of these nanoparticles with rutile nanorods' surfaces can be explained by the fact that at the end of all synthesis processes the final pH of the solution was found to be in the range of 5−5.3 (Table 1). These pH values are close to the zero point of charge (pHzpc) of TiO_2;[17] hence the van der Waals attraction between the anatase nanoparticles and the rutile nanorods is expected to be strong since the electrostatic repulsion between the particles is limited by their electrostatic surface charge density.

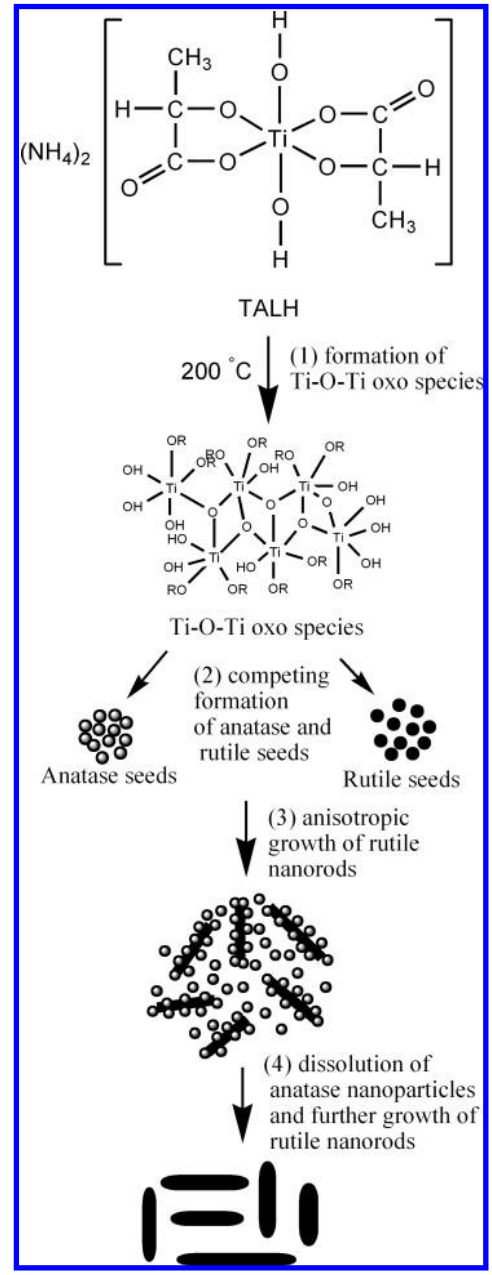

Figure 7. Proposed steps for the formation and the anisotropic growth of TiO_2 rutile nanorods.

Photocatalytic Activity. The photocatalytic activities of all newly synthesized samples were evaluated for the gas-phase decomposition of acetaldehyde, which was used as a model compound resembling harmful organic gas. With the rutile band gap of 3.0 eV (cf. Figure 5), electron−hole pairs can be generated by absorption of UV(A) light with wavelengths below 420 nm (eq 1). On the film surface the photogenerated holes react with OH^- ions or H_2O molecules, yielding highly oxidative hydroxyl ($^{\bullet}OH$) radicals (eqs 2 and 3), which are the key oxidants in the photocatalytic oxidation process.[18] These radicals quickly react with absorbed acetaldehyde, which is further oxidized to acetic acid (eqs 4−8) and finally to carbon dioxide (equations not shown) via chain radical reactions.[18b,c] The photogenerated electrons are consumed by adsorbed oxygen molecules to form superoxide radicals and/or hydrogen peroxide (eqs 9−11), which also contribute to the oxidation of acetaldehyde via the intermediate formation of $^{\bullet}OH$ radicals (eq 12). The superoxide radicals and/or hydrogen peroxide can also react

with the photogenerated holes mediating a recombination channel (eqs 13−15).

$$TiO_2 \xrightarrow{h\nu} e_{TiO_2}^- + h_{TiO_2}^+ \quad (1)$$

$$h_{TiO_2}^+ + OH^- \rightarrow {}^\bullet OH \quad (2)$$

$$h_{TiO_2}^+ + H_2O \rightarrow {}^\bullet OH + H_{aq}^+ \quad (3)$$

$$CH_3CHO + {}^\bullet OH \rightarrow CH_3C^\bullet O + H_2O \quad (4)$$

$$CH_3C^\bullet O + {}^\bullet OH \rightarrow CH_3COOH \quad (5)$$

$$CH_3C^\bullet O + O_2 \rightarrow CH_3(CO)OO^\bullet \quad (6)$$

$$CH_3(CO)OO^\bullet + CH_3CHO \rightarrow CH_3(CO)OOH + CH_3C^\bullet O \quad (7)$$

$$CH_3(CO)OOH + CH_3CHO \rightarrow 2CH_3COOH \quad (8)$$

$$e_{TiO_2}^- + O_2 \rightarrow O_2^{\bullet -} \quad (9)$$

$$O_2^{\bullet -} + H_{aq}^+ \rightarrow HO_2^\bullet \quad (10)$$

$$HO_2^\bullet + e_{TiO_2}^- + H_{aq}^+ \rightarrow H_2O_2 \quad (11)$$

$$H_2O_2 + O_2^{\bullet -} \rightarrow {}^\bullet OH + OH^- + O_2 \quad (12)$$

$$h_{TiO_2}^+ + O_2^{\bullet -} \rightarrow O_2 \quad (13)$$

$$h_{TiO_2}^+ + HO_2^\bullet \rightarrow O_2 + H_{aq}^+ \quad (14)$$

$$h_{TiO_2}^+ + H_2O_2 \rightarrow HO_2^\bullet + H_{aq}^+ \quad (15)$$

Figure 6 shows the photonic efficiencies of acetaldehyde decomposition for the different synthesized and commercial TiO_2 nanomaterials. As shown in Figure 6, the rutile nanorods decorated with 9% anatase nanoparticles (according to the Rietveld phase analysis) (RA48) exhibit a higher photocatalytic activity than pure rutile nanorods (R72 and R96) and even a higher activity than the rutile nanorods embedded in 53% anatase nanoparticles (according to the Rietveld phase analysis) (RA24). Moreover, the photocatalytic activity of RA48 was found to be higher than that of rutile nanoparticles (R25 and R34) and at least comparable to that of TiO_2 P25. The higher photocatalytic activity of rutile nanorods decorated with 9% anatase nanoparticles (RA48) as compared with that of pure rutile nanorods (R72 and R96) can be explained by the fact that anatase nanoparticles usually exhibit a higher photocatalytic activity than rutile in the case of the acetaldehyde decomposition.[8,19] Interestingly, the rutile nanorods decorated with only 9% anatase nanoparticles (RA48) show a higher photocatalytic activity than rutile nanorods embedded in anatase nanoparticles (RA24); however, the latter material has a higher content of anatase (53%). This can be explained by the fact that the conduction band edge of TiO_2 anatase is about 0.2 eV more negative than that of rutile. This is suggested to facilitate interfacial electron transfer, and the energy barrier would suppress back electron transfer. Consequently the holes left in the valence band of anatase efficiently oxidize the organic substrates, while the electrons having moved to the rutile are consumed by the reduction of oxygen. This will lead to better charge carrier separation and thus to an increase of the photocatalytic activity.[4] This charge transfer behavior between anatase and rutile is experimentally supported by photodeposition experiments of Ag[19] in similar structures and noted in many systems.[4,8] The slightly lower activity of the rutile nanorods totally covered by anatase nanoparticles as compared with that of the rutile nanorods only decorated with a smaller amount of anatase nanoparticles, however, can be explained by geometric considerations. Due to the complete coverage of the rutile rods by anatase particles, it becomes more difficult for the photogenerated electrons to be scavenged by oxygen molecules because of a blocking effect (i.e., lack of free access of molecular oxygen to the rutile surface), whereas in the case of the rutile nanorods decorated with anatase nanoparticles there is sufficient room enabling free access of molecular oxygen to the rutile surface.

Conclusions

TiO_2 rutile nanorods either decorated with anatase nanoparticles or pure have been prepared via a facile single-step hydrothermal method using commercially available aqueous solutions of titanium bis(ammonium lactate) dihydroxide (TALH) at natural pH (~8.0) without any additives. The photocatalytic activity of the investigated powders indicate that TiO_2 rutile nanorods decorated with anatase nanoparticles exhibit higher photocatalytic activity than those either embedded in anatase nanoparticles or in the absence of any anatase particles. This is readily explained by a better charge carrier separation in the case of the anatase−rutile mixtures.

Acknowledgment. We thank Dr. L. Robben (Institute of Mineralogy, Leibniz Universität Hannover) for XRD measurements and Rietveld phase analysis. T.A.K. thanks the Egyptian Ministry of Higher Education for providing him a doctoral scholarship.

References and Notes

(1) (a) Zhang, H.; Chen, G.; Bahnemann, D. W. *J. Mater. Chem.* **2009**, *19*, 5089–5121. (b) Liu, B.; Aydil, E. S. *J. Am. Chem. Soc.* **2009**, *131*, 3985–3990. (c) Song, X.-M.; Wu, J.-M.; Tang, M.-Z.; Qi, B.; Yan, M. *J. Phys. Chem. C* **2008**, *112*, 19484–19492. (d) Kandiel, T. A.; Feldhoff, A.; Robben, L.; Dillert, R.; Bahnemann, D. W. *Chem. Mater.* **2010**, DOI: 10.1021/cm903472p.

(2) Prieto-Mahaney, O. O.; Murakami, N.; Abe, R.; Ohtani, B. *Chem. Lett.* **2009**, *38*, 238–239.

(3) (a) Kim, S. J.; Lee, J. K.; Lee, E. G.; Lee, H. G.; Lee, K. S. *J. Mater. Res.* **2003**, *18*, 729–732. (b) Habibi, M. H.; Vosooghian, H. *J. Photochem. Photobiol., A* **2005**, *174*, 45–52.

(4) (a) Zachariah, A.; Baiju, K. A.; Shukla, S.; Deepa, K. S.; James, J.; Warrier, K. G. K. *J. Phys. Chem. C* **2008**, *112*, 11345–11356. (b) Li, G.; Ciston, S.; Saponjic, Z. V.; Chena, L.; Dimitrijevic, N. M.; Rajh, T.; Gray, K. A. *J. Catal.* **2008**, *253*, 105–110. (c) Miyagi, T.; Kamei, M.; Mitsuhashi, T.; Ishigaki, T.; Yamazaki, A. *Chem. Phys. Lett.* **2004**, *390*, 399–402.

(5) Wang, W.; Gu, B.; Liang, L.; Hamilton, W. A.; Wesolowski, D. *J. Phys. Chem. B* **2004**, *108*, 14789–14792.

(6) (a) Tahir, M. N.; Theato, P.; Oberle, P.; Melnyk, G.; Faiss, S.; Kolb, U.; Andreas, J.; Stepputat, M.; Tremel, W. *Langmuir* **2006**, *22*, 5209–5212. (b) Bae, E.; Ohno, T. *Appl. Catal., B: Environ.* **2009**, *91*, 634–639.

(c) Bae, E.; Murakami, N.; Ohno, T. *J. Mol. Catal. A: Chem.* **2009**, *300*, 72–79. (d) Zhang, Q.; Gao, L. *Langmuir* **2003**, *19*, 967–971. (e) Huang, Q.; Gao, L. *Chem. Lett.* **2003**, *32*, 638–639. (f) Huang, X.; Pana, C. *J. Cryst. Growth* **2007**, *306*, 117–122. (g) Dessombz, A.; Chiche, D.; Davidson, P.; Panine, P.; Chaneac, C.; Jolivet, J.-P. *J. Am. Chem. Soc.* **2007**, *129*, 5904–5909. (h) Fei, B.; Deng, Z.; Xin, H. X.; Zhang, Y.; Pang, G. *Nanotechnology* **2006**, *17*, 1927–1931.

(7) (a) Kobayashi, M.; Petrykin, V.; Kakihana, M.; Tomita, K. *J. Ceram. Soc. Jpn.* **2007**, *115*, 835–839. (b) Kobayashi, M.; Petrykin, V.; Kakihana, M. *J. Am. Ceram. Soc.* **2009**, *92*, S21–S26.

(8) Liu, Z.; Zhang, X.; Nishimoto, S.; Jin, M.; Tryk, D. A.; Murakami, T.; Fujishima, A. *Langmuir* **2007**, *23*, 10916–10919.

(9) Mendive, C. B.; Bredow, T.; Feldhoff, A.; Blesa, M.; Bahnemann, D. *Phys. Chem. Chem. Phys.* **2008**, *10*, 1960–1974.

(10) Tauc, J.; Grigorovici, R.; Vanuc, A. *Phys. Status Solidi* **1966**, *15*, 627.

(11) Möckel, H.; Giersig, M.; Willig, F. *J. Mater. Chem.* **1999**, *9*, 3051–3056.

(12) One thermal hydrolysis experiment was performed employing sealed glass ampules at 160 °C for 48 h. The isolated powder, however, was found to be a mixture of anatase and rutile (93% anatase and 7% rutile) according to the Rietveld phase analysis.

(13) Li, Y.; Fan, Y.; Chen, Y. *J. Mater. Chem.* **2002**, *12*, 1387–1390.

(14) (a) Oliver, P. M.; Wastson, G. W.; Kelsely, E. T.; Parker, S. C. *J. Mater. Chem.* **1997**, *7*, 563–568. (b) Diebold, U. *Surf. Sci. Rep.* **2003**, *48*, 53–229. (c) Barnard, A. S.; Zapol, P. *Phys. Rev. B* **2004**, *70*, 235403.

(15) Jiang, Y.; Yin, H.; Sun, Y.; Liu, H.; Lei, L.; Chen, K.; Wada, Y. *Appl. Surf. Sci.* **2007**, *253*, 9277–9282.

(16) (a) Ribeiro, C.; Vila, C.; Stroppa, D. B.; Mastelaro, V. R.; Bettini, J.; Longo, E.; Leite, E. R. *J. Phys. Chem. C* **2007**, *111*, 5871–5875. (b) Wang, Y.; Zhang, L.; Deng, K.; Chen, X.; Zou, Z. *J. Phys. Chem. C* **2007**, *111*, 2709–2714.

(17) (a) Kormann, C.; Bahnemann, D. W.; Hoffmann, M. R. *J. Phys. Chem.* **1988**, *92*, 5196–5201. (b) Pena, M.; Meng, X.; Korfiatis, G. P.; Jing, C. *Environ. Sci. Technol.* **2006**, *40*, 1257–1262. (c) Lakshminarasimhan, N.; Kim, W.; Choi, W. *J. Phys. Chem. C* **2008**, *112*, 20451–20457.

(18) (a) Kim, H.; Choi, W. *Appl. Catal., B: Environ.* **2007**, *69*, 127–132. (b) Ohko, Y.; Tryk, D. A.; Hashimoto, K.; Fujishima, A. *J. Phys. Chem. B* **1998**, *102*, 2699–2704. (c) Sopyan, I.; Watanabe, M.; Murasawa, S.; Hashimoto, K.; Fujishima, A. *J. Photochem. Photobiol., A* **1996**, *98*, 79–86. (d) Hoffmann, M. R.; Martin, S. T.; Choi, W.; Bahnemann, D. W. *Chem. Rev.* **1995**, *95*, 69–96.

(19) Kawahara, T.; Konishi, Y.; Tada, H.; Tohge, N.; Nishii, J.; Ito, S. *Angew. Chem., Int. Ed.* **2002**, *41*, 2811–2813.

JP912008K